Surface barrier for electrons in metals

P. J. Jennings,* R. O. Jones, and M. Weinert†
Institut für Festkörperforschung der Kernforschungsanlage Jülich, D-5170 Jülich, Federal Republic of Germany
(Received 14 September 1987; revised manuscript received 23 October 1987)

Density-functional calculations using the full-potential linearized augmented-plane-wave (FLAPW) film method have been used to compute the effective potential for electrons at different surfaces of Al, Ni, Cu, Ag, and W. In each case, the average of the potential parallel to the surface is reproduced well by a simple model barrier with three adjustable parameters, with relatively small variations between different metals and surfaces. FLAPW calculations have also been used to examine the effects of chemisorption on the surface barrier. The results of this work provide a basis for the analysis of low-energy-electron-diffraction fine-structure and inverse-photoemission spectra.

I. INTRODUCTION

An understanding of the interaction of an electron with a metal surface is essential for describing many surface processes, such as low-energy electron diffraction (LEED), field emission, photoemission, inverse photoemission, and surface-barrier tunneling. The variation of the potential near the metal-vacuum interface, often referred to as the "surface barrier," has been central to discussions of the electron-surface interaction for many years. It is well known from classical electrostatics that an electron outside an ideal metal surface is attracted to its image, with a potential function of the form

$$V(z)=\frac{1}{2z} . \tag{1}$$

We use Rydberg atomic units, with the metal in the half-space $z \geq 0$.

This solution is clearly unsatisfactory near the surface, where $V(z)\rightarrow -\infty$. The first quantum-mechanical attempt to go beyond this idealized picture was given by Bardeen,[1] who examined the potential barrier for the "jellium" model of a simple metal, where the ionic charges are represented by a uniform positive background. Bardeen performed approximately self-consistent Hartree-Fock calculations, assuming a local density description of correlation. His results showed that the electron-surface interaction far outside the surface ($z \rightarrow -\infty$) is described by the image form, but there are large deviations as the electron approaches the surface. Within a few atomic units of the surface, the corrections can be comparable to the image term itself, and the potential goes over smoothly to a value inside the metal characteristic of the interaction of the electron with the "exchange-correlation hole" in the bulk. This departure from the singular form of Eq. (1) is often referred to as "saturation."

More detailed calculations on the same model of the metal-vacuum interface have been performed by other authors.[2–8] Lang and Kohn[2–4] (LK) performed self-consistent density-functional calculations, with a local density description of exchange and correlation, to determine charge densities and effective potentials for an electron in the surface region. They found that the effective potential for an electron in jellium had an exponential decay as $z \rightarrow -\infty$ due to their use of the local approximation for correlation and exchange. However, when they considered the response of the surface to an external electric field they found that the potential far from the surface had the image form of Eq. (1), but with the reference plane shifted outwards from the edge of the jellium background,

$$V(z)=\frac{1}{2(z-z_I)} . \tag{2}$$

The position of the image plane ($z=z_I$) can in this case be identified with the center of mass of the induced surface charge,[3] and LK found that z_I lies 1–2 a.u. beyond the jellium edge. Appelbaum and Hamann[5] carried out a variational calculation of the electron-surface interaction, and fitted the calculation potential near the surface to a shifted image potential of the same form. They found that the position of the image plane so determined lay closer to the jellium edge than that obtained by LK. Subsequently, Ossicini *et al.*[6] carried out calculations similar to those of LK but with a nonlocal approximation for exchange and correlation. They fitted the tails of their calculated effective potentials to a shifted image potential and obtained values of z_I similar to those of Appelbaum and Hamann.

The above considerations apply to static charges. A simple physical model based on the interaction of a moving charge with its image shows that the interaction potential must also depend on the speed and angle of incidence.[7] In the context of the long-range (van der Waals) atom-surface interaction, it has been shown that the image-plane location is a function of frequency, moving closer to the jellium edge for moving charges.[8]

The picture which emerges from all the model calculations mentioned above is remarkably consistent. The potential has a (shifted) image form far from the surface, with a smooth transition to a value determined by the electron-electron interactions in the solid. In view of the importance of the surface barrier, it is not surprising that there have been numerous one-dimensional barrier models proposed for the analysis of experimental measure-

ments. Cutler and Davis[9] have summarized earlier work on these models, most of which were introduced to facilitate analytical solutions to barrier scattering problems, rather than to simulate the results of accurate calculations of the barrier shape. It is natural to ask how well model barriers can describe the actual potential barrier in real materials, and which experiments are sensitive to the barrier form.

The scattering of electrons from surfaces should provide information about the surface barrier. Experience has shown, however, that the calculated intensities in (LEED) are insensitive to assumptions about barrier shape, except at very low energies (<20 eV). In this energy range, high-resolution measurements exhibit fine structure, which we have shown to be determined principally by the surface potential barrier.[10] To analyze these spectra we have used a one-dimensional barrier model of the form

$$V(z)=\begin{cases}\dfrac{1}{2(z-z_0)}\{1-\exp[\lambda(z-z_0)]\} & \text{if } z<z_0\\ \dfrac{-U_0}{A\exp[-B(z-z_0)]+1} & \text{otherwise .}\end{cases} \tag{3}$$

Here A and B are constants determined by matching $V(z)$ and its derivative at the reference plane $z=z_0$, so that $B=U_0/A$ and $A=-1+2U_0/\lambda$. This barrier model satisfies the qualitative requirements mentioned above, and has three adjustable parameters z_0, λ, and U_0. It has an asymptotic form similar to the shifted image potential [Eq. (2)], as this is essential to fit the observed pattern of peak spacings in LEED fine structure.

The parameter z_0 may loosely be identified with the location of the image plane. Since LEED experiments are often performed with electrons which have substantial kinetic energies, z_0 will be energy dependent, and it should lie closer to the surface than the static image plane.[8] The z_0 we find is an *effective* image-plane location for generating a potential for LEED and similar phenomena. The parameter λ determines the range over which the barrier saturates. At the reference plane, the potential has the value $V(z_0)=-\lambda/2$. As $z\to\infty$ inside the solid, the model potential approaches the value U_0, the inner potential of the metal. U_0 is also a function of the electron kinetic energy, becoming smaller in magnitude as the velocity increases. For low-energy-electron-diffraction studies, U_0 is approximately equal to the sum of the Fermi energy and the surface work function. Its value decreases at higher energies as shown by studies of Bragg peak locations in LEED intensity spectra.[11]

Recently we have analyzed linearized augmented-plane-wave (LAPW) calculations of thin metal films to study the adequacy of this model for transition metal surfaces. Although the calculated potentials for W(001) and W(110) show pronounced three-dimensional features, the model of Eq. (3) was found to describe very well the averaged single-particle effective potential in the surface region.[10,12] Moreover, the results of our simulations of the LEED fine structure with this model yield barrier parameters z_0, λ, and U_0 in close agreement with those obtained by fitting the model to the results of the LAPW calculations.[10,13,14]

In view of the importance of model barriers in studying surface processes such as inverse photoemission, photoassisted field emission, and tunneling microscopy and the success of our model barrier in analyzing the LEED fine structure for W(001) and W(110) we have attempted to explore its applicability to other metal surfaces. Our aim is to model the potential seen by an external electron and we use the thin-film calculations as a guide to the form of the effective potential in the transition region close to the metal surface. We determine values of the barrier parameters by fitting the effective potentials to the model potential of Eq. (3).

In addition to the range of variation of the three parameters z_0, λ, and U_0, it is important to determine (a) the differences between the values of the parameters obtained from density-functional calculations for jellium and for real surfaces, (b) the variation in the parameters from one crystal face to another, (c) whether z_0 and λ are functions of U_0 in general, and (d) the effects of chemisorption, at monolayer coverage, on the surface-barrier structure.

The results of this study should indicate the suitability of our barrier model for simulating electron scattering processes at surfaces, and should be of direct relevance to the analysis of very-low-energy-electron-diffraction (VLEED) experiments[15] and inverse-photoemission spectra.[16–19]

In Sec. II, we outline aspects of the density-functional method, which is the basis of the work of LK and of the surface calculations described below. We show that the numerical values of the jellium potential found by LK are described well by our model barrier. In Sec. III, we describe density-functional calculations for surfaces of Al, Ni, Cu, Ag, and W using the full-potential linearized augmented-plane-wave (FLAPW) method. Section IV discusses the effects found for chemisorption, and our concluding remarks are given in Sec. V.

II. DENSITY-FUNCTIONAL CALCULATIONS FOR JELLIUM

The density-functional formalism provides a framework for calculating the total energy and density of a system of interacting electrons in an external field, $V_{\rm ext}$. It reduces the many-particle problem to the self-consistent solution of single-particle equations of Hartree type

$$[-\nabla^2+V_{\rm eff}(\mathbf{r})]\psi_i(\mathbf{r})=\epsilon_i\psi_i(\mathbf{r}) . \tag{4}$$

The effective potential in this equation can be written

$$V_{\rm eff}(\mathbf{r})=\Phi_{\rm es}(\mathbf{r})+V_{\rm xc}(\mathbf{r})+V_{\rm ext}(\mathbf{r}) , \tag{5}$$

where $\Phi_{\rm es}$ is the electrostatic potential, found by solving Poisson's equation, and $V_{\rm xc}$ is the exchange-correlation potential. The density is found from

$$n(\mathbf{r})=\sum_{i=1}^{n} f_i\,|\,\psi_i(\mathbf{r})\,|^2 , \tag{6}$$

where the f_i are appropriate occupation numbers, and

the calculation is repeated until self-consistency is obtained. The calculation is simplified greatly if V_{xc} has a local dependency on the density, and this approximation is very common.

In the calculations of Lang and Kohn,[4] the external field is that of a uniform positive charge in the half-space $z > 0$, and Eqs. (4)–(6) have the single spatial parameter, z. They were solved for electron gases of densities corresponding to r_s values from 2 to 6, yielding values of the inner potential, work function, and effective potential in each case. The results are plotted for $r_s = 2$, 4, and 6 in Fig. 1, together with our fit to their curves using the model of Eq. (3). The fit is performed by fixing the value of U_0 to the value determined by LK, and optimizing the parameters λ and z_0. We have emphasized the region close to the surface in performing this fit because the LK calculations are known to be inaccurate as $z \to -\infty$ due to their use of the local density approximation for correlation and exchange.

Figure 1 shows that the fit is very good, and the values of U_0, z_0, and λ obtained are presented in Table I. We also show the classical image potential with its origin at the center of mass of the induced surface charge as determined by LK from the linear response of the system to an additional external field. It is clear that significant saturation sets in as the electron approaches within 5 a.u. of the surface, although the shifted image form is adequate far away.

The values of z_0 which we have determined by fitting the LK data to our model are significantly closer to the surface than the classical-image-plane locations determined by LK, but similar to those of Appelbaum and Hamann[5] and Ossicini *et al.*[6] These differences may arise from the different ways in which the long-range exchange and correlation effects are treated in each of these calculations.[5]

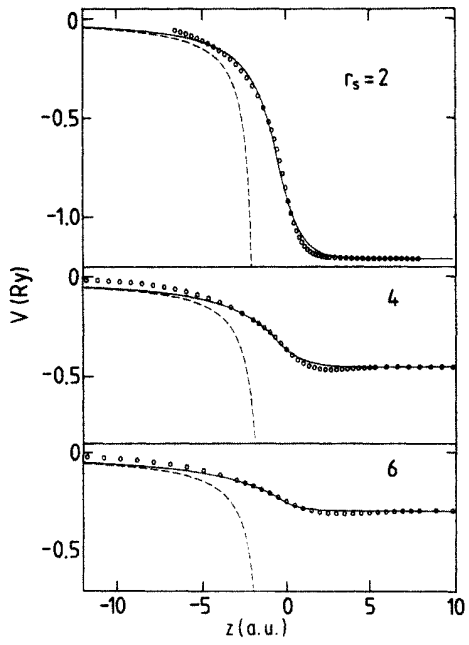

FIG. 1. Comparison of the effective potential energy for an electron in the vicinity of jellium surfaces with $r_s = 2, 4, 6$. The open circles represent the calculated results of Lang and Kohn (Ref. 4), the solid curve is the fit obtained using Eq. (3), and the dashed curve is the classical image potential for the static case.

TABLE I. Surface-barrier parameters for the jellium model (Rydberg atomic units) determined by fitting the effective potentials of LK (Ref. 4). The parameters z_0, λ, and U_0 are defined by Eq. (3) and z_J is the position of the jellium edge.

r_s	$z_0 - z_J$	λ	U_0
2	−0.70	1.25	1.21
4	−0.65	0.62	0.46
6	−0.20	0.46	0.28

The location of the effective image plane z_0 relative to the jellium edge varies inversely with r_s, so that metals with a high density of conduction electrons (small r_s) produce a stronger image force on a charge at the same distance from the jellium edge. Similar trends are apparent for the other parameters. A small value of λ indicates strong saturation of the barrier, and we note that metals with a low density of conduction electrons (large r_s) have the smallest values of λ. The calculated value of the inner potential U_0 varies approximately inversely with r_s.

These results show that the saturated image barrier provides a satisfactory picture of the surface barrier in the jellium model, with reasonable value of the parameters. However, the jellium approach neglects the atomic structure, which produces different work functions and inner potentials for different crystal faces. It is also unlikely to be adequate for transition and rare-earth metals which have strongly bound d and f conduction electrons. Many important metals fall into these categories, and it is necessary to test the model potential against more realistic calculations of the effective potential at the metal-vacuum interface.

III. DENSITY-FUNCTIONAL CALCULATIONS FOR THIN FILMS

Several methods exist to solve the (self-consistent) density-functional equations for a surface, and accurate solutions require that the spatial variations of the charge and potential (including the ionic charge) be treated correctly. A surface has intrinsically low symmetry, and approximations commonly used for the bulk, such as the muffin-tin approximation, would give rise to large and incorrect dipoles. It would be advantageous to treat a semi-infinite solid, as in the case of jellium, but accurate methods for calculating the electronic structure are not currently available. The alternatives are to treat a finite number of layers (of the order of 5–20) in supercell or thin-film geometries. In the supercell geometry, one considers a bulk unit cell comprising a number of atomic layers plus empty or "vacuum" layers, repeated periodically throughout space. The film geometry assumes periodicity in two dimensions only, and treats the vacuum region correctly. The screening length of the electrons is comparable to the interlayer spacing, so that a small number

of layers can represent the surface reliably. Experience has shown that the thin-film approximation is well justified for many properties, including such delicate questions as the energetics of surface reconstructions.

The thin-film FLAPW method used here is described in detail elsewhere.[20] In this method, space is divided into spheres surrounding the atomic sites, a vacuum region outside the film, and the interstitial region. The potential, density, and wave functions are expressed in the "natural" representations for each region: products of spherical harmonics and numerical radial functions inside the spheres, plane waves in the interstitial, and products of 2D plane waves and z-dependent functions in the vacuum region. The approach is variational, and its accuracy can be improved systematically. While the Coulomb potential is treated without shape approximation, we assume the local density approximation for exchange and correlation. The differences between these calculations and others which make additional approximations are generally unimportant, provided that the main anisotropies in the density and potential are taken self-consistently into account.

To make the comparisons between the barrier model and the surface calculations, the planar average of the total potential is needed. While the planar average of the *total* potential is well defined, this average is quite deep due to the nuclear attraction. In the spirit of LEED-type calculations, the potential inside the muffin-tin spheres should not be included in the determination of the surface barrier, and the straightforward solution is to average over the interstitial region alone. This has the disadvantage, however, that the averaged potential is discontinuous in slope at the sphere boundaries.

For present purposes, the contribution to the average arising from the spheres can then be found using any convenient, physically motivated method, and various ways can be found which result in a smooth average while removing the main contributions from the spheres. In previous work,[10,12] the charge density and potential of the surface were approximated by a plane-wave expansion assumed valid everywhere inside the film plus muffin-tin contributions inside the spheres. In this representation, the average potential is simply the average of the plane-wave portion.

In the present calculations, the plane-wave representation of the density and potential is assumed valid only in the interstitial region, while inside the spheres the actual charge density is used. This change in representation requires a different method of solving Poisson's equation, and the simple average of the plane-wave-extended potential is not the same as determined before.[10,12] The solution of Poisson's equation used[21] exploits the fact that the potential outside the spheres depends on the density inside only through the multipole moments of the density. Once the potential is obtained outside the spheres, a boundary-value problem is solved inside the spheres using the actual density to generate the Coulomb potential in rapidly converging representations appropriate to the various regions of space.

The planar-averaged potential used for comparison with the barrier model was obtained by assuming a plane-wave representation for the Coulomb potential in the interstitial region:

$$V_I(\mathbf{r})=\sum_{\mathbf{G}} V(\mathbf{G})e^{i\mathbf{G}\cdot\mathbf{r}}+\sum_{\mathbf{G}_\parallel} w(\mathbf{G}_\parallel)\exp(i\mathbf{G}_\parallel\cdot\mathbf{r}_\parallel)\cosh(G_\parallel z) + c_0\left[\left(\frac{D}{2}\right)^2-z^2\right] . \tag{7}$$

This form assumes reflection symmetry about the center of the film, and the constant $c_0=2\pi\tilde{\rho}(0)$ is related to the $\mathbf{G}=\mathbf{0}$ Fourier coefficient of the (pseudo-) charge density[20,21] inside the film of thickness D. While this form of the potential is the same as used before,[10,12] its value *inside* the spheres can differ markedly because of the different methods used to solve Poisson's equation.

The potential V_I can be expanded straightforwardly into a spherical-harmonic representation on each sphere α (with radius S_α),

$$V_I(\mathbf{S}_\alpha)=\sum_{l,m} V^I_{lm}(S_\alpha)Y_{lm}(\hat{S}_\alpha) , \tag{8}$$

using the standard Rayleigh expansion for a plane wave and a similar expansion[20] valid for plane waves with complex wave vectors to treat the $\exp(i\mathbf{G}_\parallel\cdot\mathbf{r}_\parallel)\cosh(G_\parallel z)$ terms. To obtain the full potential inside the spheres, one then solves the boundary-value problem

$$V_\alpha(\mathbf{r}_\alpha)=\int_{S_\alpha} d\mathbf{r}\,\rho_\alpha(\mathbf{r})G(\mathbf{r}_\alpha,\mathbf{r})-\frac{S_\alpha^2}{4\pi}\oint_{S_\alpha} d\Omega\, V_I(\mathbf{S}_\alpha)\frac{\partial G}{\partial n} , \tag{9}$$

where $G(\mathbf{r}_\alpha,\mathbf{r})$ is the electrostatic Green's function for a sphere and $\partial G/\partial n$ is its normal derivative. Here we have solved Poisson's equation inside the spheres, but neglecting the volume term (i.e., setting the density inside the spheres to zero). This is equivalent to replacing the density inside the spheres by bulk jellium, since the latter gives no electrostatic contribution. Note, however, that the full anisotropy of the density inside the spheres is taken into account in determining the interstitial potential and the boundary-value problem. The modified potential inside the spheres is then

$$\tilde{V}_\alpha(\mathbf{r}_\alpha)=\sum_{l,m}\left[\frac{r_\alpha}{S_\alpha}\right]^l V^I_{lm}(S_\alpha)Y_{lm}(\hat{S}_\alpha) \tag{10}$$

for the Coulomb potential plus the exchange-correlation potential corresponding to the interstitial plane-wave-extended charge density.

The averaged potential $\bar{V}(z)$ is given by

$$\bar{V}(z)=\frac{1}{A}\int d\mathbf{r}_\parallel \tilde{V}(\mathbf{r}_\parallel,z) , \tag{11}$$

where A is the surface unit-cell area and $\tilde{V}$ is the modified potential given above. These averages can all be calculated simply (only the $m=0$ spherical harmonics contribute). Three-dimensional plots of the full and modified potentials for a (10) plane of the W(001) surface are shown in the left frames of Figs. 2(a) and 2(b), respectively, and contour plots of the modified potential in Fig. 3. Even though the full potential is dominated by the at-

tractive nuclear Coulomb potential, its three-dimensional nature is still evident. As discussed above, the modified potential removes most of the effects of the muffin-tin contribution. The planar averaged potential is shown in Fig. 4(a). The expanded plot for $-5 \leq z \leq 1$ shows that the model barrier [Eq. (3), dashed line] provides a very good representation of the planar average in this range.

The results of fitting the model barrier to the averaged thin-film effective potentials are presented in Table II. The same fitting procedure was used as for the jellium effective potentials discussed in Sec. II. The barrier parameters obtained for Al closely resemble the results of the jellium calculations for $r_s = 2$ (see Table I). The effective image plane for Al(001) lies 1.03 a.u. beyond the jellium edge compared with 0.70 a.u. for $r_s = 2$. The values of λ and U_0 are also similar in both calculations despite the considerable differences in the computational models used to calculate the effective potentials. This result indicates that the jellium approach is adequate for free-electron metals although it neglects the effects of crystal structure on the barrier.

For transition metals we observe much stronger deviations from the jellium picture. All cases listed in Table II have effective image planes located between 0.69 and 1.65 a.u. from the jellium edge, corresponding roughly to $r_s \leq 2$ in the jellium model of LK (see Table I). The values of z_0, λ, and U_0 are larger for the more densely packed faces of W(110) and Cu(001) than for the more open faces W(001) and Cu(110). The heavier metals such as Ag and W also have larger values of z_0 because of the increased atomic radii. There is a general trend for z_0 and λ to increase for metals with a large U_0, but this trend is not as uniform as in the jellium model, because factors such as the lattice structure, the atomic radius, and the electronic configuration also influence the values of the barrier parameters for transition metals.

The difference between the values given in Table II for W(001) and W(110) and those reported previously[10,12,14]

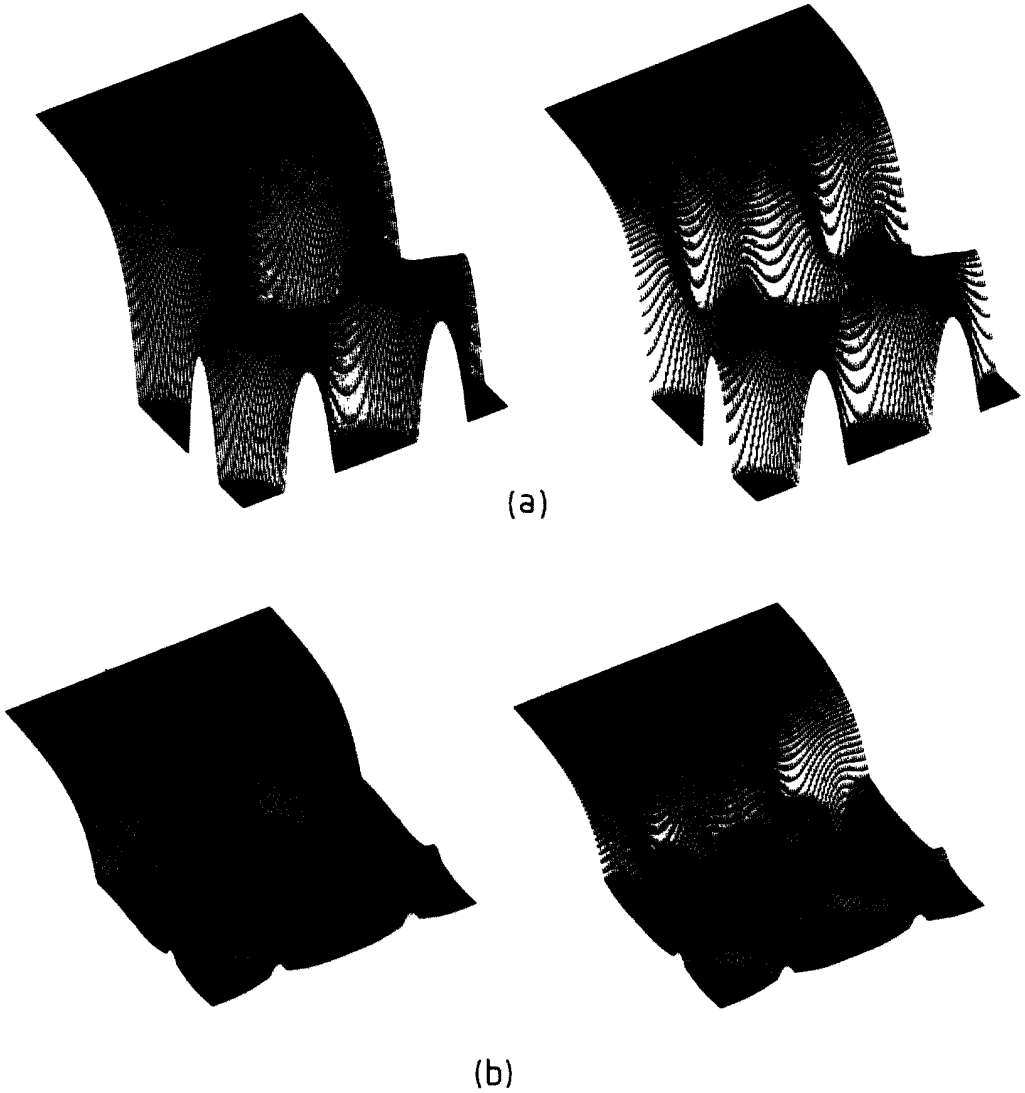

FIG. 2. Three-dimensional plots of (a) the total effective potential and (b) the modified potential in a (10) plane for W(001). The right frame shows the corresponding results for $p(1\times1)$-2H chemisorption.

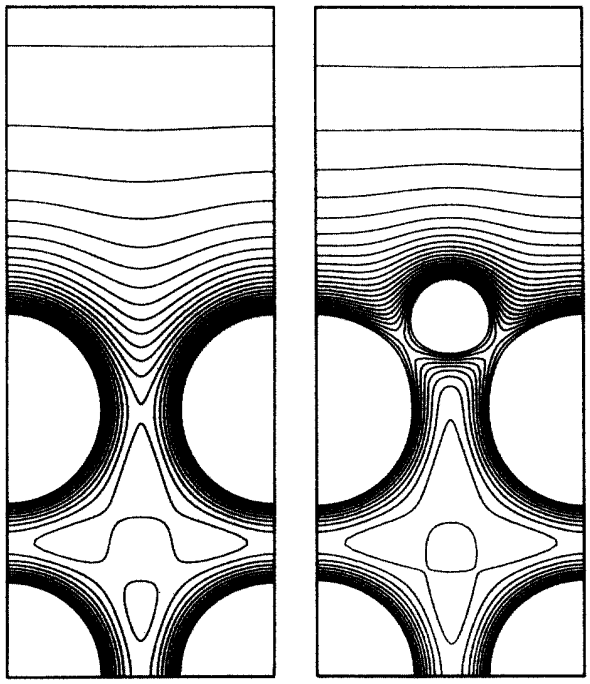

FIG. 3. Contour plots (spacing 0.075 Ry) of the modified potential for W(001) [(10) plane, left] and for the same plane for W(001)$p(1\times1)$-2H.

arise from the different definitions of the "modified" potentials. The differences between the two faces are very similar in the two calculations, and the qualitative conclusions are unchanged. The uncertainties in z_0,λ of ~0.2 and in U_0 of ~0.1 give a range of uncertainty to be expected for such analyses.

The barrier parameters obtained from the thin-film calculations are in qualitative agreement with those obtained empirically by fitting measured spectra for a number of metal surfaces (see Table III). In general the values of z_0, λ, and U_0 are reasonably close to those in Table II, but the numbers derived from LEED fine-structure analysis are lower than those obtained from the thin-film calculations. These differences are consistent with dynamical effects arising from the higher kinetic energies of the electrons used in LEED experiments. The empirical results for W(001) and W(110) are the most reliable, as they are based on a detailed analysis of a large amount of high-quality data. The other LEED results should be regarded as preliminary until they have been checked against a larger data base.

It is encouraging that the photoemission and inverse-photoemission results of Smith and Chen[18] using the model barrier of Eq. (3) lead to a value of z_0 in Cu(110) (-2.4 a.u.) in satisfactory agreement with our value (-2.17 a.u.). They also obtain the same value for Ni(110) and Cu(110), consistent with our results for the (001) surfaces of these elements. It should be noted, however, that the position of the reference plane, z_0, depends on the barrier model assumed. Thörner and Borstel,[19] for example, assumed the model of Rundgren and Malmström[26] in analyzing inverse photoemission data from Cu(001). This has the form

$$V(z)=\begin{cases}\dfrac{1}{2(z-z_0)}+\dfrac{V_1}{(z-z_0)^2} & \text{if } z<z_1'<z_0\\ U_0\ , & z>z_2'\end{cases} \tag{12}$$

with a polynomial interpolation between these two regions. While the optimum value of z_0 (1.93 a.u.) is simi-

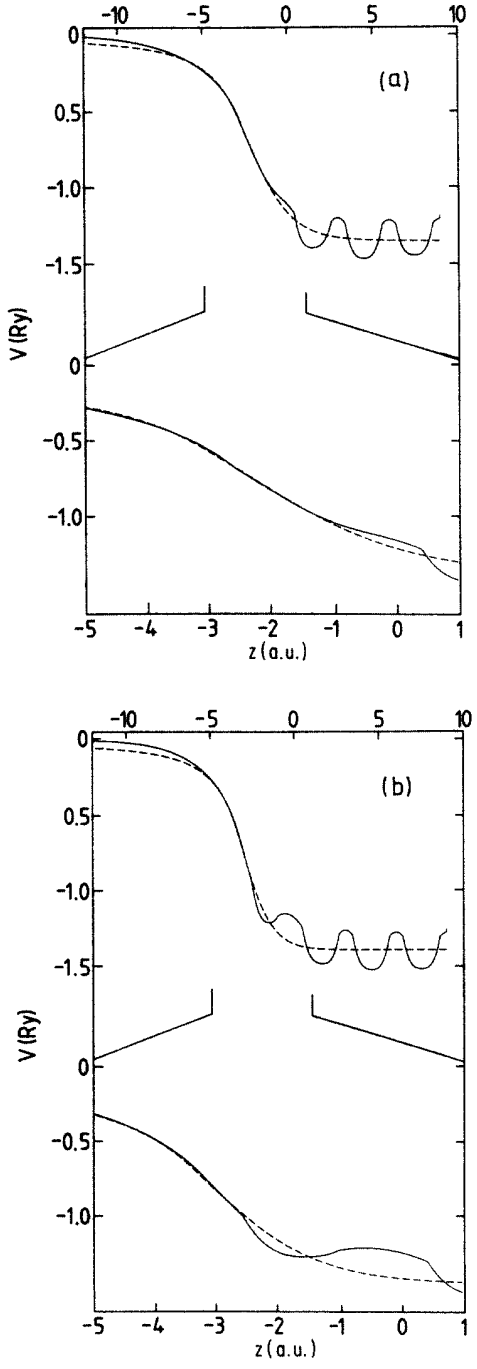

FIG. 4. Planar average of the modified potential for the (10) plane of W(001); (a) clean surface, (b) with $p(1\times1)$ hydrogen chemisorption.

TABLE II. Barrier parameters obtained by fitting the model barrier potential to the averaged thin-film effective potentials (Rydberg atomic units). The variables are defined in Eq. (3) and the location of the jellium edge is taken as half the interlayer spacing normal to the surface above the topmost layer of atoms.

Crystal plane	z_0-z_J	z_0	λ	U_0
Al(001)	−1.03	−2.95	1.00	1.08
Ni(001)	−0.72	−2.38	1.20	1.19
Cu(001)	−0.69	−2.40	1.15	1.12
Cu(110)	−0.96	−2.17	1.05	1.11
Ag(110)	−0.96	−2.35	0.97	1.01
W(001)	−1.65	−3.15	0.98	1.35
W(110)	−1.14	−3.28	1.03	1.45

lar to the values in Table III, it is not surprising that they are not identical.

These results indicate values of the barrier parameters appropriate for analyzing LEED and inverse-photoemission spectra. For all of the transition metals listed in Table II we find that $|z_0-z_J|\sim 1$ a.u., $\lambda\sim 1$ a.u.$^{-1}$, and $U_0\sim 1$ Ry. Using these starting values, the optimal barrier parameters can be obtained by fitting the experimental data as described elsewhere.[11]

IV. CHEMISORPTION EFFECTS ON BARRIER STRUCTURE

We have studied previously the effects of hydrogen and oxygen adsorption on the LEED fine structure of W(110).[27] if we consider that chemisorption produces a thin dielectric layer of thickness δ and dielectric constant ϵ on the metal surface, the classical image analysis shows that the potential energy of an electron a distance z from the metal surface is given by

$$V(z)\sim \frac{-1}{2|z-(z_0+\delta)|}\left[1-\frac{2\delta}{(\epsilon+1)|z-(z_0+\delta)|}\right] \quad \text{for } \delta \ll |z| \ . \tag{13}$$

As $z\to-\infty$ or $\epsilon\to\infty$ this result reduces to the image form, shifted outwards from the substrate surface by a distance $|z_0+\delta|$. The presence of the dielectric layer therefore shifts the reference plane farther from the jellium edge of the metal. However, the correction term arising from the presence of the dielectric film on the surface reduces the strength of the image force relative to the clean metal, and the outward shift of z_0 will be less than that predicted by the jellium model. The inner potential of the metal will also change on chemisorption, and this change should be similar to the measured change in the work function for that surface. The saturation parameter λ can be expected to change correspondingly.

TABLE III. Empirical values of the barrier parameters determined by fitting LEED fine-structure, photoemission, and inverse-photoemission data (Rydberg atomic units).

Crystal plane	z_0	λ	U_0	References
W(001)	−2.90	0.90	1.00	10,13
W(110)	−3.10	0.90	1.05	14
Ni(001)	−2.30		1.05	22
Ni(110)	−2.4	0.9	0.85	18
Cu(001)	−2.35	1.05	0.85	22–25
Cu(110)	−2.4	0.9	0.85	18
Cu(111)	−2.60	1.10	0.90	23–25

It is important to have a good understanding of the expected changes in the barrier parameters as a basis for VLEED studies of chemisorption. This is a promising experimental technique which has been used recently to study several adsorption systems.[15,27] In our study of oxygen and hydrogen adsorption on W(110) we found that VLEED was very sensitive to the adsorption sites of the adatoms. LEED computations at very low energies are relatively simple, but the analysis requires a good model of the surface barrier. We found, however, that the major effects were due to changes in the scattering properties of the surface layer, so that there was no need to optimize completely the barrier parameters for the chemisorbed system.

For this reason we have analyzed a thin-film calculation of hydrogen on W(001) to determine the shifts occurring in the barrier parameters on chemisorption. These results should indicate an appropriate choice of barrier parameters for VLEED studies of chemisorption on transition metals. The calculations for the saturated W(001)$p(1\times1)$-2H system were carried out as described above for clean surfaces. The H-W interlayer spacing was determined from total energy FLAPW calculations,[28] and the calculated structural and electronic properties are in good agreement with available experimental data. The potentials for the hydrogen-covered surface are shown alongside the corresponding results for the clean surface in Figs. 2–4. The hydrogen atoms strongly modify the potential in the surface region, resulting in different barrier parameters.

The results in Table IV show that the effective-image-plane location moves outwards by 0.3 a.u., which is considerably less than the shift in the jellium edge of 1.24 a.u., since the dielectric layer reduces the image force and suppresses the outward shift of the reference plane. The inner potential increases from 1.35 to 1.40 Ry, consistent with the measured increase of the work function of W(001) of 0.90–0.95 eV as a result of hydrogen chemisorption.[29] The calculated work-function change is 0.95 eV. The difference between the work-function change and the change in U_0 is due to both the averaging and fitting procedures.

The results of this analysis confirm our previous conclusions[27] that chemisorption on a metal surface produces a small outward shift of the effective image plane and corresponding changes in λ and U_0. This picture should be valid for other chemisorption systems and provide a basis for estimating changes in barrier parameters for use in analyzing VLEED experiments.

V. CONCLUSIONS

We have shown that our simple, three-parameter barrier model provides a good fit to the averaged, one-

TABLE IV. Barrier parameters for clean W(001) and H/W(001) obtained by fitting the model barrier to the averaged thin-film potentials (Rydberg atomic units). The location of the jellium edge, z_J, is calculated in accordance with the approach of LK (Ref. 2).

Crystal plane	z_J	z_0	λ	U_0
W(001)	−1.50	−3.15	0.98	1.35
H/W(001)	−2.74	−3.45	1.25	1.40

dimensional effective potential for an electron in the vicinity of metal-vacuum interfaces. The parameters can be identified with important physical properties of the barrier, and can be optimized independently by fitting thin-film calculations or experimental data. The resulting values of the parameters z_0, λ, and U_0 obtained by both procedures are in close agreement.

By comparing the calculated values of the barrier parameters for several transition metals, we have shown that the characteristic values of these parameters are similar to those for free-electron metals with $r_s \leq 2$. Structural effects are evident, with different values of the parameters being obtained for different planes of the same crystal. In general, z_0 and λ increase as U_0 increases, but the pattern is complicated by the dependence of these parameters on the atomic radii, crystal structure, and electronic structure of the metal. A study of the adsorption of hydrogen on W(001) indicates that the effective-image-plane location z_0 moves outward from the metal during adsorption and that the other barrier parameters λ and U_0 change in parallel with the work-function change.

These results provide a semiquantitative picture of the one-dimensional potential energy barrier for electrons at the metal-vacuum interface. They can be used to select appropriate values of the barrier parameters for analyzing electronic processes which involve surface-barrier effects. Such processes include LEED fine-structure analysis, VLEED studies of chemisorption, inverse-photoemission spectroscopy, and surface-barrier tunneling.

ACKNOWLEDGMENTS

We thank N. D. Lang and A. Liebsch for helpful discussions during the preparation of this paper. One of us (M.W.) was supported in part by the Alexander von Humboldt Foundation and by the Division of Materials Sciences, U.S. Department of Energy (Contract No. DE-AC02-76CH00016).

*Permanent address: School of Mathematical and Physical Sciences, Murdoch University, Murdoch WA 6150, Australia.

†Permanent address: Department of Physics, Brookhaven National Laboratory, Upton, NY 11973.

[1]J. Bardeen, Phys. Rev. **49**, 653 (1936); **58**, 727 (1940).

[2]For a review of this work, see N. D. Lang, Solid State Phys. **28**, 225 (1973). The energy zero in the work of Lang and Kohn is different from that in the present work, where we adopt the vacuum level.

[3]N. D. Lang and W. Kohn, Phys. Rev. B **7**, 3541 (1973).

[4]N. D. Lang and W. Kohn, Phys. Rev. B **1**, 4555 (1970).

[5]J. A. Appelbaum and D. R. Hamann, Phys. Rev. B **6**, 1122 (1972).

[6]S. Ossicini, C. M. Bertoni, and P. Gies, Europhys. Lett. **1**, 661 (1986).

[7]J. Harris and R. O. Jones, J. Phys. C **6**, 3585 (1973); **7**, 3751 (1974).

[8]See, for example, E. Zaremba and W. Kohn, Phys. Rev. B **13**, 2270 (1976); A. Liebsch, *ibid.* **33**, 7249 (1986).

[9]P. H. Cutler and J. C. Davis, Surf. Sci. **1**, 194 (1964).

[10]R. O. Jones, P. J. Jennings, and O. Jepsen, Phys. Rev B **29**, 6474 (1984).

[11]P. J. Jennings and S. M. Thurgate, Surf. Sci. **104**, L210 (1981).

[12]O. Jepsen and R. O. Jones, Phys. Rev. B **34**, 6695 (1986).

[13]J.-M. Baribeau, J.-D. Carette, P. J. Jennings, and R. O. Jones, Phys. Rev. B **32**, 6131 (1985).

[14]P. J. Jennings and R. O. Jones, Phys. Rev. B **34**, 6699 (1986).

[15]M. Lindroos, H. Pfnür, P. Feulner, and D. Menzel, Surf. Sci. **180**, 237 (1987).

[16]S. L. Hulbert, P. D. Johnson, M. Weinert, and R. F. Garrett, Phys. Rev. B **33**, 760 (1986).

[17]M. Ortuño and P. M. Echenique, Phys. Rev. B **34**, 5199 (1986).

[18]N. V. Smith, Phys. Rev. B **32**, 3549 (1985); C. T. Chen and N. V. Smith, *ibid.* **35**, 5407 (1987).

[19]G. Thörner and G. Borstel, Appl. Phys. **41**, 99 (1986).

[20]E. Wimmer, H. Krakauer, M. Weinert, and A. J. Freeman, Phys. Rev. B **24**, 864 (1981); M. Weinert, E. Wimmer, and A. J. Freeman, *ibid.* **26**, 4571 (1982); L. F. Mattheiss and D. R. Hamann, *ibid.* **33**, 823 (1986).

[21]M. Weinert, J. Math. Phys. **22**, 2433 (1981).

[22]P. J. Jennings, S. M. Thurgate, and G. L. Price, Surf. Sci. **13**, 1180 (1982). The barrier model of Ref. 24 was used in this analysis, so that no value of λ was obtained.

[23]P. J. Jennings, unpublished analysis of the data in Refs. 24 and 25.

[24]R. E. Dietz, E. G. McRae, and R. L. Campbell, Phys. Rev. Lett. **45**, 1280 (1980).

[25]S. Thurgate and G. Hitchen, Appl. Surf. Sci. **24**, 202 (1985).

[26]J. Rundgren and G. Malmström, J. Phys. C **10**, 4671 (1977).

[27]P. J. Jennings and R. O. Jones, Surf. Sci. **176**, 691 (1986).

[28]M. Weinert, A. J. Freeman, and S. Ohnishi, Phys. Rev. Lett. **56**, 2295 (1986).

[29]A. H. Smith, R. A. Barker, and P. J. Estrup, Surf. Sci. **126**, 327 (1984).

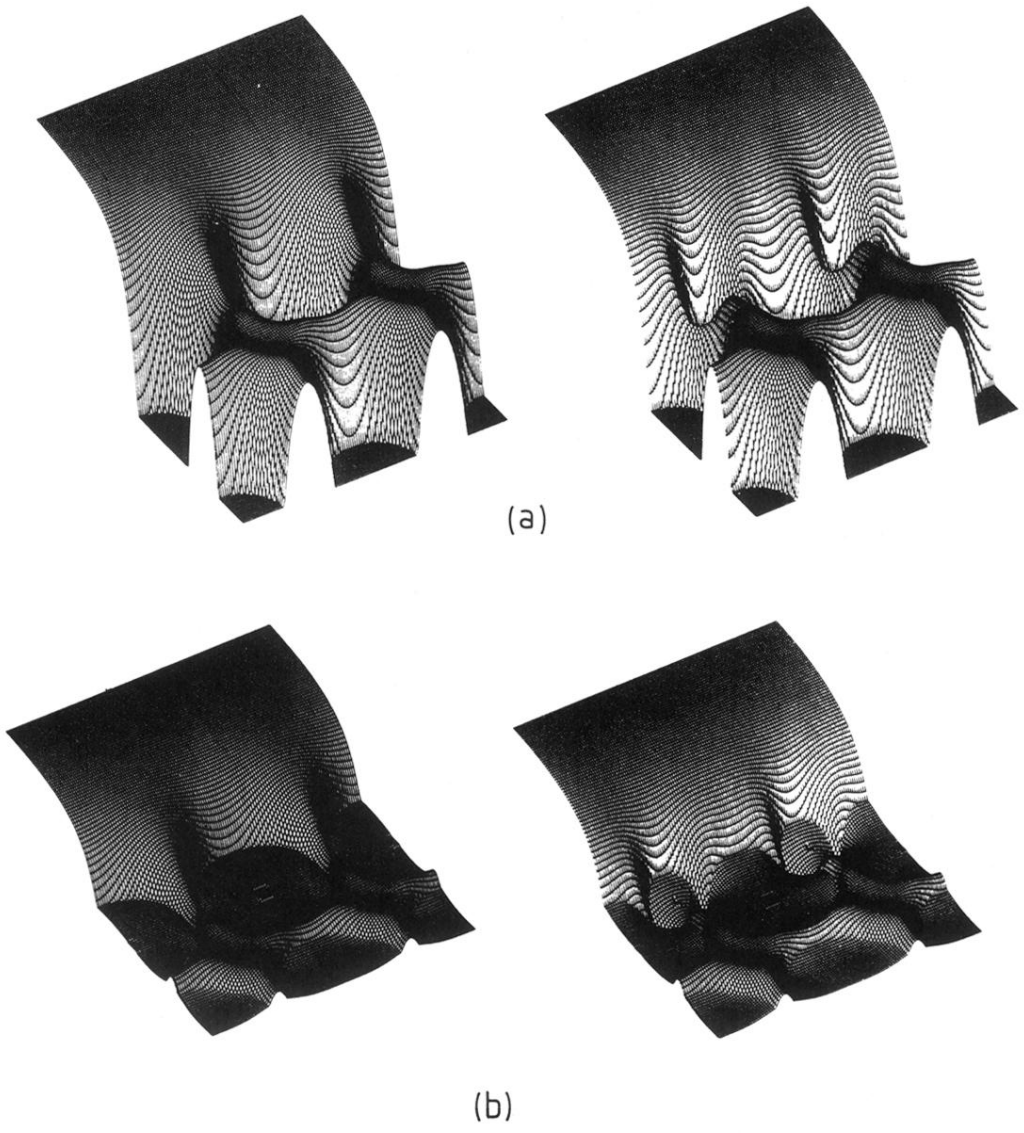

FIG. 2. Three-dimensional plots of (a) the total effective potential and (b) the modified potential in a (10) plane for W(001). The right frame shows the corresponding results for $p(1\times1)$-2H chemisorption.